Nonequilibrium Modeling of Two-Phase Critical Flows in Tubes

F. Dobran
Applied Science Department,
New York University,
New York, NY 10003
Assoc. Mem. ASME

A nonequilibrium two-phase flow model is described for the analysis of critical flows in variable diameter tubes. Modeling of the two-phase flow mixture in the tube is accomplished by utilizing a one-dimensional form of conservation and balance equations of two-phase flow which account for the relative velocity and temperature differences between the phases. Closure of the governing equations was performed with the constitutive equations which account for different flow regimes, and the solution of the nonlinear set of six differential equations was accomplished by a variable step numerical procedure. Computations were carried out for a steam–water mixture with varying degrees of liquid subcooling and stagnation pressures in the vessel upstream of the tube and for different tube lengths. The numerical results are compared with the experimental data involving critical flows with variable liquid subcoolings, stagnation pressures, and tube lengths, and it is shown that the nonequilibrium model predicts well the critical flow rate, pressure distribution along the tube, and the tube exit pressure.

1 Introduction

1.1 Relevance of the Problem. The rupture of a vessel or pipe containing a subcooled liquid at high pressure may produce a rapid depressurization of the fluid. When this occurs, the liquid flashes soon after its pressure reaches the saturation condition and thereafter flows as a two-phase mixture. With a sufficiently high stagnation pressure upstream of the break, the flow through the break reaches the critical flow condition whereby the flow rate becomes a maximum and independent of the conditions downstream of the break. The critical flow rate through the broken pipe or vessel depends on the state of the fluid upstream of the break and on the characteristics of the break itself.

Knowledge of the critical mass flow rate through the ruptured vessel or pipe is important not only for predicting the depressurization history of the fluid in the vessel and the flow through the broken pipe, but also for calculating the forces produced by the expanding jet on the pipe or vessel and on the surrounding equipment that may be located in the vicinity of the jet. For this purpose, it is important to estimate reliably the two-phase fluid characteristics exiting from a ruptured vessel or piping system.

1.2 Previous Work and Objectives of the Paper. Many models have been proposed in the past for modeling critical two-phase flows; reviews have been written by Wallis [1], Saha [2], Isbin [3], Richter [4], and Dobran [5], among others.

The modeling of two-phase critical flows in ducts can be carried out by the homogeneous (equilibrium) model or by a wide variety of nonequilibrium models. The homogeneous model assumes a thermodynamic equilibrium between the phases and it provides good results for the critical flow rate when there is a sufficient time for the two phases to reach equilibrium as might, for example, occur in long tubes. In short tubes, however, this condition may not be satisfied and the homogeneous model is usually replaced by a nonequilibrium model. The nonequilibrium effects are associated with the relative velocity and temperature differences between the phases and are, thus, functions of the flow regime. The homogeneous model offers no heat transfer resistance and, consequently, the thermal relaxation time is equal to zero. Since the real flow has a finite relaxation time, a departure from the homogeneous flow will occur whenever the two-phase mixture accelerates rapidly or the residence time of a fluid particle in the flow channel is small. For flows in short pipes or nozzles, it may be assumed that the time associated with the phase change is short, and an assumption of a frozen flow (or a constant quality flow) may be reasonable [6].

The early nonequilibrium models were empirical in nature and cannot be used with confidence in the extrapolation of the critical flow parameters. By using separate conservation and balance equations of each phase and solving these equations along the tube, such that the critical flow becomes dependent on the history of flow up to the critical point, the modeling has proved more successful. The advantage of this approach is that the thermal and mechanical nonequilibrium between the phases can be described to a large degree of complexity, but at the expense of a great deal of information which is necessary to complete the model description (such as initial nucleation site density and bubble diameter, interphase friction characteristics and heat transfer, criteria which account for different flow regimes, etc.), and it is possible to reach a point of diminishing returns where the results obtained from such a model are worse than when using a simpler model which requires less input information. Modeling of critical flows utilizing the conservation and balance equations of each phase [4, 5, 7–11] requires the specification of initial conditions which may be in the form of the initial velocities of the two phases, the initial bubble population density and size (or void fraction), and the liquid superheat. Since complete specification of the model also requires specification of tube wall friction, interphase friction, interphase heat transfer coefficient, and flow regime which at the present are incompletely understood, there should be very good reason indeed for modeling critical flows utilizing separate conservation and balance equations of each phase.

The purpose of this paper is to present a nonequilibrium model for the analysis of two-phase critical flows which is based on the separate conservation and balance equations for each phase and to substantiate the analytical predictions with the experimental data. The reasons for developing such a model are twofold: (1) to develop modeling capabilities for two-phase critical flows, and (2) to obtain detailed flow conditions at the tube exit that can be used to study the two-phase flow jet on the outside of the tube. The two-phase critical flow model contains a number of improvements over the models developed in [4, 11]. It uses correct forms of the governing

Contributed by the Heat Transfer Division for publication in the JOURNAL OF HEAT TRANSFER. Manuscript received by the Heat Transfer Division May 1, 1985.

equations and improved correlations for the constitutive equations. With these improvements, the proposed critical flow model is expected to be applicable over a larger range of liquid stagnation conditions and duct geometric conditions.

2 Description of a Two-Phase Critical Flow Model

The two-phase critical flow model will allow for the hydrodynamic and thermal nonequilibrium between the phases, where the former nonequilibrium arises from the velocity and pressure differences between the phases and the latter for the temperature difference between the liquid and gas. To simplify the model it will be assumed that the gas phase is in a thermal equilibrium (at a local saturation pressure) and that both phases are at the same pressure at any cross section of the duct. Furthermore, it will be also assumed that the critical flow through a tube can be modeled by one-dimensional, steady-state forms of the conservation and balance equations for two-phase flow.

2.1 Steady-State, One-Dimensional Forms of Conservation and Balance Equations for Two-Phase Flow. The steady-state, one-dimensional forms of the conservation and balance equations for two-phase flow may be found in Wallis [12], Collier [13] and Dobran [5]. These are:

Conservation of Mass Equations:

From the gas and liquid mass flow rates

$$M_G = \alpha \rho_G A u_G = xM \tag{2.1}$$

$$M_L = (1-\alpha)\rho_L A u_L = (1-x)M \tag{2.2}$$

and equations of state

$$\rho_G = \rho_G(P) \tag{2.3}$$

$$\rho_L = \rho_L(h_L, P) \tag{2.4}$$

we may obtain

$$\rho_G A u_G \frac{d\alpha}{dz} + \alpha A u_G \frac{d\rho_G}{dP}\frac{dP}{dz} + \alpha \rho_G A \frac{du_G}{dz} - M\frac{dx}{dz} = -\alpha \rho_G u_G \frac{dA}{dz} \tag{2.5}$$

$$-\rho_L A u_L \frac{d\alpha}{dz} + (1-\alpha)Au_L\left(\frac{\partial \rho_L}{\partial P}\right)_{h_L}\frac{dP}{dz} + (1-\alpha)\rho_L A\frac{du_L}{dz} + M\frac{dx}{dz} + (1-\alpha)Au_L\left(\frac{\partial \rho_L}{\partial h_L}\right)_P \frac{dh_L}{dz} = -(1-\alpha)\rho_L u_L \frac{dA}{dz} \tag{2.6}$$

where z is the distance along the tube and is defined in Fig. 1.

Momentum Equations:

$$\alpha \rho_G A u_G \frac{du_G}{dz} = -\alpha A \frac{dP}{dz} - F_{LG}A - F_{wG}A - \eta(u_G - u_L)M\frac{dx}{dz} - \rho_G g \alpha A \cos\theta \tag{2.7}$$

$$(1-\alpha)\rho_L A u_L \frac{du_L}{dz} = -(1-\alpha)A\frac{dP}{dz} + F_{LG}A - F_{wL}A - (1-\eta)(u_G - u_L)M\frac{dx}{dz} - \rho_L g(1-\alpha)A\cos\theta \tag{2.8}$$

In the above equations F_{LG} is the drag force per unit volume acting on the liquid phase in the direction of flow, and in the opposite direction on the gas phase; F_{wG} and F_{wL} are the drag forces per unit volume exerted by the tube wall on the gas and liquid, respectively. The terms containing η in equations (2.7) and (2.8) represent the effect of phase change and it appears that this value is close to 1/2 [12]. For horizontal flow $\cos\theta = 0$ and for vertical upflow $\cos\theta = 1$.

Nomenclature

a = interfacial area/unit volume of the mixture
A = tube flow cross-sectional area
C_D = drag coefficient, defined by equations (2.19) and (2.20)
Cf_i = interfacial friction coefficient, defined by equations (2.15)–(2.17)
Cp = specific heat at constant pressure
C_{VM} = coefficient defined by equation (2.28)
d = average bubble diameter, defined by equation (2.23)
D = tube diameter
f = frictional coefficient
F_{LG} = interfacial drag force defined by equation (2.9)
F_{wL} = drag force at the wall defined by equation (2.35)
g = gravitational constant
G = mass flux
h = enthalpy
$\tilde{h}$ = heat transfer coefficient
k = thermal conductivity
K = tube inlet loss coefficient in equation (2.47)
L = tube length
M = mass flow rate
N = bubble density
Nu = Nusselt number
P = pressure
Pr = Prandtl number = $\mu Cp/k$
$\dot{Q}_L$ = heat transfer rate from liquid to gas, defined by equation (2.29)
Re = Reynolds number
S = slip ratio = u_G/u_L
T = temperature
u, u^* = axial velocity in the tube; $u^* = \rho_0' u/G_0$
x = quality
X = vector of dependent variables in equation (2.60)
z = distance along the tube, see Fig. 1
α = gas volumetric fraction or void fraction
Δ = virtual mass coefficient, defined by equation (2.27)
η = energy redistribution coefficient in equations (2.10) and (2.11)
μ = viscosity
ξ = viscous drag coefficient, defined by equation (2.14)
ρ = density
σ = surface tension
τ = shear stress
ϕ = two-phase frictional multiplier, defined by equation (2.38)

Subscripts

a = annular flow
b = bubbly flow
FLO = friction liquid only
G = pertains to the gas phase
GO = gas only
i = pertains to initial point
L = pertains to the liquid phase
LO = liquid only
0 = at the tube inlet
0′ = stagnation state, see Fig. 2
sat = saturation
sub = subcooling
sup = superheating
w = wall

For bubbly and separated flows, where the liquid phase flows adjacent to the tube wall, $F_{wG} = 0$, and it will be assumed in the present model. The interphase drag force F_{LG} may be modeled as follows [5, 14, 15]

$$F_{LG} = \xi_{GG}(u_G - u_L) + \Delta_{GG}\left(u_G \frac{du_G}{dz} - u_L \frac{du_L}{dz}\right) \tag{2.9}$$

where $\xi_{GG} \geq 0$ is the viscous drag coefficient and $\Delta_{GG} \geq 0$ is the virtual mass coefficient which accounts for the relative acceleration between the phases. Substituting equation (2.9) into equations (2.7) and (2.8) results in the following momentum equations for gas and liquid

$$[\rho_G u_G \alpha A + \Delta_{GG} u_G A] \frac{du_G}{dz} + [-A u_L \Delta_{GG}] \frac{du_L}{dz} + [\alpha A] \frac{dP}{dz} + [\eta M(u_G - u_L)] \frac{dx}{dz} = -A\xi_{GG}(u_G - u_L) - \rho_G g \alpha A \cos\theta \tag{2.10}$$

$$[-\Delta_{GG} u_G A] \frac{du_G}{dz} + [\rho_L u_L (1-\alpha) A + \Delta_{GG} u_L A] \frac{du_L}{dz} + [(1-\alpha)A] \frac{dP}{dz} + [(1-\eta)M(u_G - u_L)] \frac{dx}{dz} = A\xi_{GG}(u_G - u_L) - \rho_L g (1-\alpha) A \cos\theta - F_{wL} A \tag{2.11}$$

Energy Equations. A control volume energy balance on the two-phase flow mixture in the tube of length dz with an adiabatic wall and similarly on the liquid phase yields

$$M\left[h_{LG} + \frac{1}{2}(u_G^2 - u_L^2)\right]\frac{dx}{dz} + \left[xM \frac{dh_G}{dP}\right]\frac{dP}{dz} + [xMu_G] \frac{du_G}{dz} + [(1-x)Mu_L] \frac{du_L}{dz} + [(1-x)M] \frac{dh_L}{dz} + Mg\cos\theta = 0 \tag{2.12}$$

$$M\left[h_{LG} + \frac{1}{2}(u_G^2 - u_L^2)\right]\frac{dx}{dz} = \frac{d\dot{Q}_L}{dz} \tag{2.13}$$

where use was made of $h_{LG} = h_G - h_L$ and the equations of state and conservation of mass, equations (2.1)–(2.4). $d\dot{Q}_L/dz$ in the above equation denotes the heat transfer rate per unit tube length from the liquid to the gas.

The two-phase flow nonequilibrium model consists of six equations, (2.5), (2.6), and (2.10)–(2.13), which must be solved for six unknowns: α, x, u_G, u_L, P, and h_L. Before this can be done, however, the constitutive equations for ξ_{GG}, Δ_{GG}, F_{wL}, and $d\dot{Q}_L/dz$ must be specified. The tube geometry is assumed to be known, i.e., $A = A(z)$, and the mass flow rate M is treated as a parameter and is determined as described below. The thermodynamic properties $h_G(P)$, $\rho_G(P)$, $\rho_L(h_L, P)$, $(\partial\rho_L/\partial P)_{h_L}$, and $(\partial\rho_L/\partial h_L)_P$ can be determined for a specific substance from thermodynamic tables.

2.2 Constitutive Equations. As the two-phase flow mixture expands through the tube its flow regime may change from bubbly flow at low void fractions to the annular flow at high void fractions. At intermediate void fractions the flow regime is usually classified as churn-turbulent [12]. The flow regime will be accounted in the model through the specification of constitutive equations for the viscous drag ξ_{GG}, virtual mass Δ_{GG}, for the interfacial heat transfer rate expressed by $d\dot{Q}_L/dz$, and for the viscous drag at the tube wall F_{wL}. These constitutive equations are known reasonably well for bubbly and annular flows only. For the churn-turbulent flow regime, however, it will be assumed that the above constitutive equations can be determined by interpolation.

2.2.1 Viscous Drag Coefficient ξ_{GG}. The viscous drag coefficient ξ_{GG} appearing in equation (2.9) accounts for the interphase friction in the bulk of the flow. Realizing that F_{LG} represents the interfacial shear stress times the interfacial perimeter and divided by the flow area, it follows that

$$\xi_{GG} = \frac{2Cf_i}{D}\sqrt{\alpha}\,\rho_G |u_G - u_L| \tag{2.14}$$

where Cf_i is the interfacial friction coefficient and is given for bubbly, annular, and churn-turbulent flows as [5, 12, 16]

$$Cf_i = \frac{3}{8} C_{D_{1-\alpha}} (1-\alpha)^3 \sqrt{\alpha} \frac{\rho_L}{\rho_G} \frac{D}{d}; \quad 0 < \alpha \leq \alpha_b \tag{2.15}$$

$$Cf_i = 0.079\,\mathrm{Re}_G^{-0.25}\left[1 + 24(1-\sqrt{\alpha})\left(\frac{\rho_L}{\rho_G}\right)^{1/3}\right]; \quad \alpha_a \leq \alpha < 1 \tag{2.16}$$

$$Cf_i = Cf_{ib} + \left(\frac{Cf_{ib} - Cf_{ia}}{\alpha_b - \alpha_a}\right)(\alpha - \alpha_b); \quad \alpha_b < \alpha < \alpha_a \tag{2.17}$$

where Cf_{ib} is evaluated from equation (2.15) at $\alpha = \alpha_b$ and Cf_{ia} is found from equation (2.16) at $\alpha = \alpha_a$. In equation (2.15) $C_{D_{1-\alpha}}$ is the bubble drag coefficient, which may be determined from the knowledge of a single bubble drag coefficient C_D [12], i.e.,

$$C_{D_{1-\alpha}} = C_D (1-\alpha)^{-4.7} \tag{2.18}$$

$$C_D = \frac{24}{\mathrm{Re}}(1 + 0.15\,\mathrm{Re}^{0.687}); \quad \mathrm{Re} \leq 1000$$
$$C_D = 0.44; \quad \mathrm{Re} > 1000 \tag{2.19}$$

The Reynolds numbers Re in equation (2.19) and Re_G in equation (2.16) are defined as follows

$$\mathrm{Re} = \frac{\rho_L d(1-\alpha)|u_G - u_L|}{\mu_L}$$
$$\mathrm{Re}_G = \frac{\rho_G D|u_G - u_L|}{\mu_G} \tag{2.20}$$

where d is the average bubble diameter, which may be determined from the bubble number density N and interfacial area per unit volume a, i.e.,

$$\alpha \equiv \frac{\pi}{6} N d^3 \tag{2.21}$$

$$a \equiv \pi N d^2 \tag{2.22}$$

$$d \equiv \frac{6\alpha}{a} \tag{2.23}$$

2.2.2 Interfacial Area Per Unit Volume a. For bubbly flow regime, the interfacial area a may be found from equations (2.21) and (2.22), and for annular flow it follows from the definition. Hence

$$a = N\pi\left(\frac{6\alpha}{N\pi}\right)^{2/3}; \quad 0 < \alpha \leq \alpha_b \tag{2.24}$$

$$a = \frac{4}{D}\sqrt{\alpha}; \quad \alpha_a \leq \alpha < 1 \tag{2.25}$$

$$a = a_b + \left(\frac{a_b - a_a}{\alpha_b - \alpha_a}\right)(\alpha - \alpha_b); \quad \alpha_b < \alpha < \alpha_a \tag{2.26}$$

where a_b is evaluated from equation (2.24) at $\alpha = \alpha_b$ and a_a from equation (2.25) at $\alpha = \alpha_a$.

2.2.3 Virtual Mass Coefficient Δ_{GG}. The virtual mass coefficient Δ_{GG} appears in equation (2.9) and it is known reasonably well only for the bubbly flow. It is given by the expression

$$\Delta_{GG} = \alpha \rho_L C_{VM} \tag{2.27}$$

where C_{VM} appears to have the form [17]

$$C_{VM} = 0.3 \tanh(4\alpha) \tag{2.28}$$

2.2.4 Interfacial Heat Transfer $d\dot{Q}_L/dz$. The interfacial

heat transfer rate from the liquid to the gas per unit tube length can be expressed as follows:

$$\frac{d\dot{Q}_L}{dz} \equiv \tilde{h}\, aA\,(T_L - T_G) \tag{2.29}$$

where $\tilde{h}$ is the interfacial heat transfer coefficient and is modeled according to the flow regime [5, 18]. Hence

$$\mathrm{Nu} = \frac{\tilde{h}d}{k_L} = 2 + 0.6\ \mathrm{Re}_b^{1/2}\mathrm{Pr}_L^{1/3}; \qquad 0 < \alpha \le \alpha_b \tag{2.30}$$

$$\mathrm{Nu} = \frac{\tilde{h}D\sqrt{\alpha}}{k_G} = 0.023\ \mathrm{Re}_{Ga}^{0.8}\,\mathrm{Pr}_G^{0.4}; \qquad \alpha_a \le \alpha < 1 \tag{2.31}$$

$$\tilde{h} = \tilde{h}_b + \frac{(\tilde{h}_b - \tilde{h}_a)}{(\alpha_b - \alpha_a)}\,(\alpha - \alpha_b); \qquad \alpha_b < \alpha < \alpha_a \tag{2.32}$$

where $\tilde{h}_b$ is determined from equation (3.30) at $\alpha = \alpha_b$ and $\tilde{h}_a$ from equation (2.31) at $\alpha = \alpha_a$. The Reynolds numbers in the above equations are given as

$$\mathrm{Re}_b = \frac{\mathrm{Re}}{1-\alpha} = \frac{\rho_L d\,|u_G - u_L|}{\mu_L} \tag{2.33}$$

$$\mathrm{Re}_{Ga} = \frac{\rho_G D\sqrt{\alpha}}{\mu_G}\,|u_G - u_L| \tag{2.34}$$

2.2.5 Wall Friction F_{wL}. The drag force per unit volume of the mixture which is exerted by the tube wall on the liquid F_{wL} can be expressed in terms of the wall shear stress τ_w, i.e.,

$$F_{wL} = \frac{4}{D}\,\tau_w = -\left(\frac{dP}{dz}\right)_{\text{wall friction}} \tag{2.35}$$

and it will be modeled by the Chisholm correlation [19] since it fits the advanced empirical correlation curves of Baroczy (cit. [13]) quite well and accounts for the effect of mass flux on the frictional pressure gradient. The correlation is expressed by the following set of equations

$$F_{wL} = -\phi_{LO}^2\left(\frac{dP}{dz}\right)_{\text{FLO}} \tag{2.36}$$

$$\left(\frac{dP}{dz}\right)_{\text{FLO}} = \frac{4}{D} f_{LO}\,\frac{G^2}{2\rho_L} \tag{2.37}$$

$$\phi_{LO}^2 = 1 + (Y^2 - 1)[Bx^{(2-n)/2}(1-x)^{(2-n)/2} + x^{2-n}] \tag{2.38}$$

where f_{LO} is the single-phase frictional coefficient determined from

$$f_{LO} = \frac{16}{\mathrm{Re}_{LO}}; \quad \mathrm{Re}_{LO} = \frac{GD}{\mu_L} \le 2000 \tag{2.39}$$

$$f_{LO} = 0.079\ \mathrm{Re}_{LO}^{-0.25}; \quad \mathrm{Re}_{LO} > 2000 \tag{2.40}$$

n is the power in the friction factor–Reynolds number relationship ($n = 0.25$ for the Blasius equation), and

$$Y^2 = \frac{\left(\frac{dP}{dz}\right)_{GO}}{\left(\frac{dP}{dz}\right)_{LO}} = \frac{f_{GO}}{f_{LO}}\,\frac{\rho_L}{\rho_G} \tag{2.41}$$

Y	G	B
$Y \le 9.5$	≤ 500	4.8
	$500 < G < 1900$	$2400/G$
	≥ 1900	$55/G$
$9.5 < Y < 28$	≤ 600	$520/(YG^{0.5})$
$Y \ge 28$	> 600	$21/Y$
		$\dfrac{15{,}000}{(Y^2G^{0.5})}$

(2.42)

In equation (2.41) f_{GO} is determined from equations similar to equations (2.39) and (2.40), but involving the gas properties.

The utilization of the constitutive equations described above requires the specification of void fractions α_b and α_a where the flow regime changes from bubbly to churn-turbulent and from churn-turbulent to annular, respectively. From experimental data [12, 13] it may be generally assumed that $\alpha_b \simeq 0.3$ and $\alpha_a \simeq 0.8$.

2.3 Initial Conditions. The solution of the ordinary differential equations described in Section 2.1 depends on the initial conditions. As shown in Fig. 1, the fluid in the vessel at $z = 0$ is assumed to be at the stagnation state and it may be a single-phase liquid or a two-phase mixture. Referring to Fig. 2, the *liquid subcooling* is determined from the information on the stagnation state $0'$

$$\Delta T_{\text{sub}} = T_{\text{sat}}(P_{0'}) - T_{0'} \tag{2.43}$$

As the subcooled liquid expands it does not in general begin to flash at the saturation pressure corresponding to its stagnation temperature, but at a lower pressure than can be characterized by the liquid superheating which is defined as follows

$$\Delta T_{\text{sup}} = T_{0'} - T_{\text{sat}}(P(z_i)) \tag{2.44}$$

The degree to which the liquid superheats depends on its nucleation characteristics, such as on the amount of dissolved gas present in the liquid and on the rate of depressurization, among other factors. This superheat is usually found to be a few degrees Celsius and will be determined from the following correlation [20]

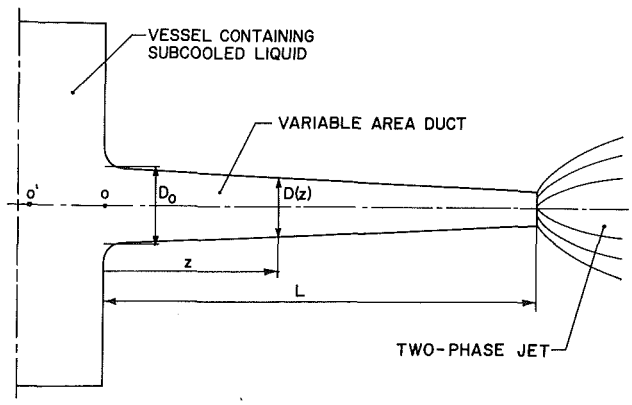

Fig. 1 Two-phase flow discharging through a variable area duct

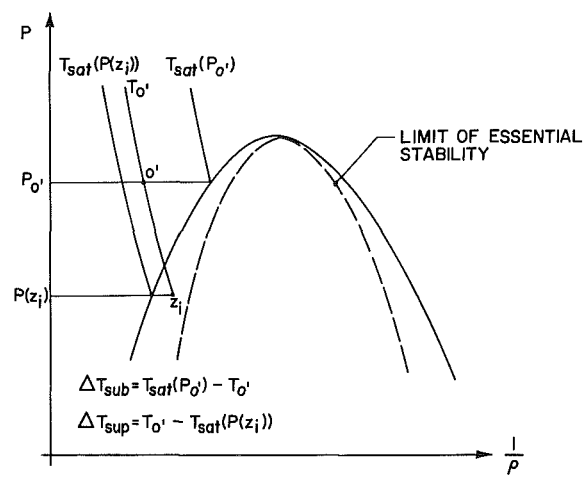

Fig. 2 Representation of subcooled and superheated liquid states on the pressure-volume diagram

$$P(z_i) = P_{sat}(T_0') - C\,\sigma^{1.5}\left(\frac{T_0'}{T_{crit}}\right)^{13.73}/(k_B T_{crit}) \tag{2.45}$$

where $C = 0.08$.

The initial conditions for the two-phase flow model described above are determined by first locating the position in the tube and the state of fluid at this position where the liquid reaches a specified amount of superheat. This initial position is found by the following procedure:

(*a*) Based on the given stagnation pressure P_0' and liquid subcooling ΔT_{sub}, find from equation (2.43)

$$T_0' = T_{sat}(P_0') - \Delta T_{sub} \tag{2.46}$$

(*b*) Using T_0' in equation (2.45), determine $P(z_i)$.

(*c*) From the Bernoulli and conservation of mass equations, i.e.,

$$P_0' = P(z_i) + (1+K)\rho_0' \frac{1}{2} u(z_i)^2 + 4\frac{f}{D} z_i \rho_0' \frac{1}{2} u(z_i)^2 \tag{2.47}$$

$$GA = \rho_0' u(z_i) A(z_i) = G_0 A_0 \tag{2.48}$$

it can be shown that

$$z_i = \frac{D(z_i)}{4f}\left[\frac{2\rho_0'[P_0' - P(z_i)]}{G_0^2} - (1+K)\right]\left[\frac{A(z_i)}{A_0}\right]^2 \tag{2.49}$$

where K is the tube entry loss coefficient and is about 0.3 for the radiused entry. The frictional coefficient f is given by

$$\frac{1}{\sqrt{4f}} = -0.86 \ln\left[\frac{\epsilon}{3.7D} + \frac{2.51}{\mathrm{Re}\sqrt{4f}}\right]; \quad \mathrm{Re} = \frac{GD}{\mu_L} \geq 4000$$

$$= \frac{16}{\mathrm{Re}}; \quad \mathrm{Re} < 4000 \tag{2.50}$$

where ϵ/D is the relative tube roughness.

The initial conditions at $z = z_i$ required to solve the differential equations are, therefore, specified as follows:

1 With the given initial nucleation site density N_i and diameter of nuclei d_i, it follows from equation (2.21) that

$$\alpha_i = \frac{\pi}{6} N_i d_i^3 \tag{2.51}$$

2 Since the quality $x = M_G/M$, it follows from equations (2.1) and (2.2) that

$$x_i = \frac{1}{1 + \dfrac{\rho_0'}{\rho_G}\dfrac{1-\alpha_i}{\alpha_i}\dfrac{1}{S_i}} \tag{2.52}$$

where $S_i = u_{Gi}/u_{Li}$ is the initial slip; it may be assumed to be equal to one.

3 From equations (2.1) and (2.52) we have

$$u_{Gi} = \frac{x_i M}{\alpha_i \rho_G A(z_i)} \tag{2.53}$$

4 The liquid velocity is found from S_i and equation (2.53), i.e.,

$$u_{Li} = u_{Gi}/S_i \tag{2.54}$$

5 The initial pressure is found from equation (2.45)

$$P_i = P(z_i) \tag{2.55}$$

6 The liquid enthalpy at $z = z_i$ is determined from the saturated liquid enthalpy at $P(z_i)$ (see Fig. 2) and from the liquid superheating, hence

$$h_{Li} = h_{Lsat}(P(z_i)) = Cp_L[T_0' - T_{sat}(P_i)] \tag{2.56}$$

where Cp_L may be evaluated at P_i.

Equations (2.51)–(2.56) specify a set of initial conditions for the two-phase flow model described in Sections 2.1 and 2.2. To close this model, however, it is also necessary to specify constitutive equations for the bubble density N and the initial size of nucleation centers. Ardron [21] provided a transport equation for N, while Richter [4] and Dobran [5] assumed a constant value of N and found that the critical flow parameters are not very sensitive to a tenfold variation in this number. In view of this and other studies described in detail in [5], it will be assumed that

$$N = N_i = 10^{11}\ 1/\mathrm{m}^3 \tag{2.57}$$

$$d_i = 5 \times 10^{-5}\ \mathrm{m} \tag{2.58}$$

2.4 Solution Procedure. The system of differential equations represented by equations (2.5), (2.6), (2.10), (2.11), (2.12), and (2.13) can be written in the following vector form

$$A^* \frac{dX}{dz} = B^* \tag{2.59}$$

where X is the vector of dependent variables, i.e.,

$$X = (\alpha, x, u_G, u_L, P, h_L)^T \tag{2.60}$$

and where the coefficients of matrix A^* and vector B^* depend on the dependent variables. The solution of the above system of equations can be accomplished by utilizing the initial conditions specified by equations (2.51)–(2.56) in terms of the tube geometry (tube length and flow cross-sectional area), fluid stagnation conditions (pressure and subcooling), and the total mass flow rate M. To determine the *critical flow rate* it is necessary and sufficient that [22]

$$\Delta = 0 \quad \text{and} \quad n_i = 0, \quad i = 1, \ldots, 6 \tag{2.61}$$

where $\Delta = \det(A^*)$ is the determinant of A^*, and n_i is the determinant obtained by replacing the ith column of A^* by the column vector B^*. The critical flow in the tube is, then, obtained by searching for that value of the mass flow rate M which will yield the conditions specified by equation (2.61) at the end of the tube.

The system of differential equations with the initial conditions discussed above was programmed for the numerical solution into a computer program which is fully discussed in [5]. Basically, the numerical integration is accomplished by a variable step Runge–Kutta procedure on the basis of a global error specification. The program automatically determines the critical mass flow rate and it has built-in thermodynamic property data tables.

3 Results and Discussion

In this section the numerical results obtained by the critical two-phase flow model discussed in the previous section are presented and compared with the steam–water experimental data of saturated and subcooled liquid discharging from a vessel through tubes of different lengths.

A comparison of the predicted critical mass fluxes with the experimental data of [23] is illustrated in Fig. 3. This comparison involves stagnation pressures from 1 to 3 MPa and subcoolings up to 40°C, and tube length-to-diameter ratios $L/D = 10 - 287.6$ with $D = 0.0125$ m. As can be seen from Fig. 3, the predicted critical mass fluxes are within ±10 percent of the experimental values, and for the subcooled liquid case with $L/D = 10$ the critical flow rates tend to be underestimated.

The predicted and experimental pressure distribution along the tube are shown in Figs. 4–6. Figures 4 and 5 show a comparison for the situation of a saturated liquid in the vessel, while Fig. 6 shows this comparison for the case of subcooled liquid with $L/D = 97$. As can be seen from these figures, the predicted pressure distributions along the tube are, overall, in a very good agreement with the data. A slight underprediction

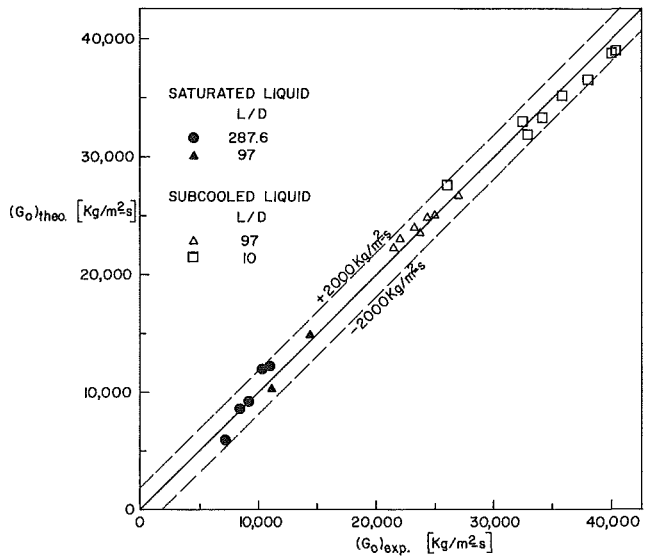

Fig. 3 Comparison of predicted and experimental mass fluxes

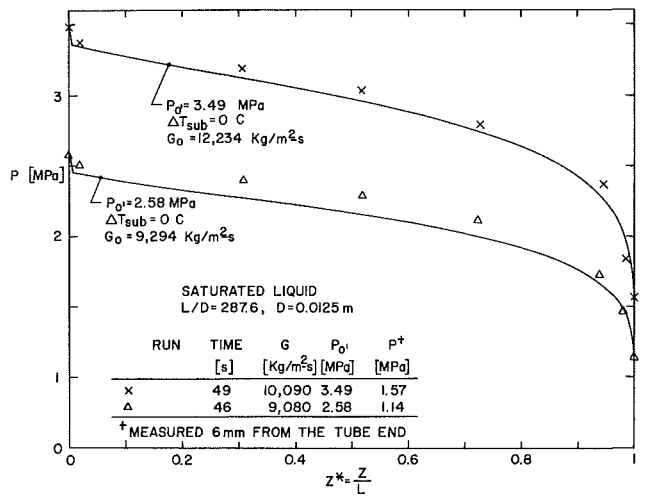

Fig. 4 Comparison of the predicted pressure distribution along the tube with the experimental data of saturated liquid

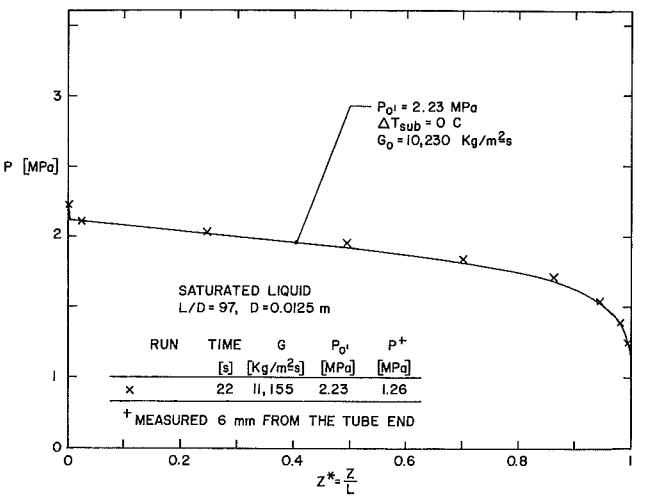

Fig. 5 Comparison of the predicted pressure distribution along the tube with the experimental data of saturated liquid

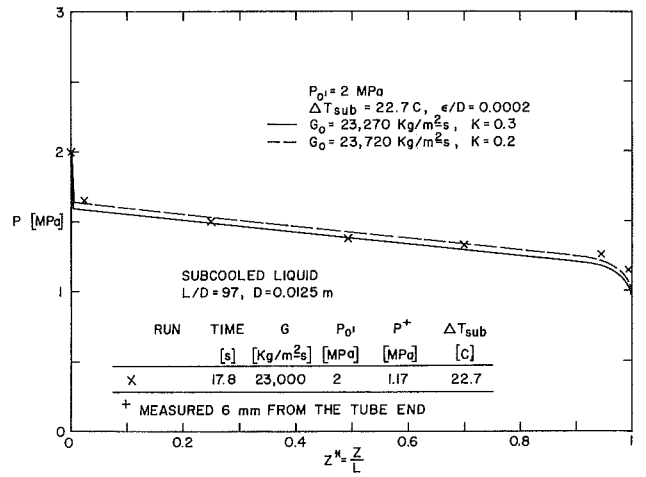

Fig. 6 Comparison of the predicted pressure distribution along the tube with the experimental data of subcooled liquid

of the data for the saturated liquid case with $L/D = 287.6$ in Fig. 4 may be attributed to the error in the specification of initial conditions in the model, since the tube entrance frictional pressure losses and two-dimensional effects may be of importance in inducing the local nucleation characteristics in the liquid which are different from the ones modeled through the simple relations as described in Section 2. In the case of subcooled liquid discharging through tubes the pressure distribution is also sensitive to the relative tube roughness and tube entrance loss coefficient as shown in Fig. 6. Accurate measurements of the tube exit pressure in critical two-phase flow situations do not appear to exit, but as Figs. 4–6 illustrate, the pressure measurements 6 mm from the tube end agree within 10 percent with the experimental data and the model predictions of the steep pressure variations near the tube exit are in accord with the data. However, for the situation [23] corresponding to the saturated liquid case discharging through a pipe with $L/D = 287.6$ the total (static and dynamic) pressure of 2.2 MPa was measured at 0.5 D from the tube exit in the jet expansion region. Using the computed values of pressure and void fraction at the tube exit for this run [5], it may be shown that the total exit pressure is 2.263 MPa which agrees closely with the experimental value of 2.2 MPa. To test further the credibility of the analytical model, a pressure transducer was inserted 0.5 mm from the tube exit [24] for the situation of saturated liquid with $L/D = 100$, $P_0' = 2.13$ MPa, and $P_0' = 2.02$ MPa. The measured pressures at this location were 0.98 and 0.934 MPa, whereas the computed exit pressures turn out to be 1.005 and 0.947 MPa, respectively.

Figures 7 and 8 illustrate the numerical results of the void fraction, quality, velocity, and liquid subcooling distributions along the tube with $L/D = 97$ and for saturated and subcooled conditions of liquid in the vessel. For the saturated liquid case in Fig. 7, the void fraction, quality, and vapor and liquid velocities increase along the tube and show a steep rise close to the tube end where the critical flow point is located. Although an initial slip ratio of 1.2 was assumed, it has no effect on the subsequent evolution of gas and liquid velocities. These velocities are also almost equal to each other, with the gas velocity being larger than the liquid velocity and this difference increasing slightly toward the end of the tube. This, of course, implies a mechanical equilibrium between the phases but not the thermal equilibrium as attested by the distribution of the liquid superheat ΔT_{sup}, which substantially increases toward the tube end where the accelerational effects tend to increase. These nonequilibrium effects also increase in shorter tubes [5].

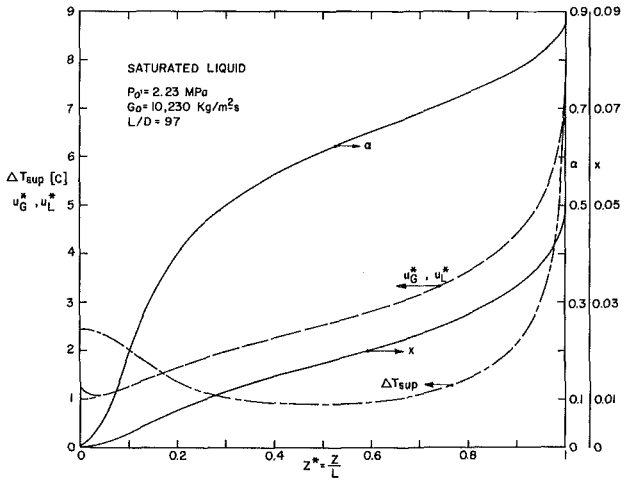

Fig. 7 Numerical results for saturated liquid and *L/D* = 97

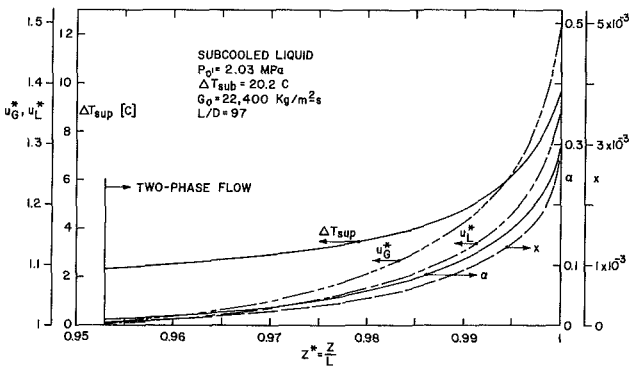

Fig. 8 Numerical results for subcooled liquid and *L/D* = 97

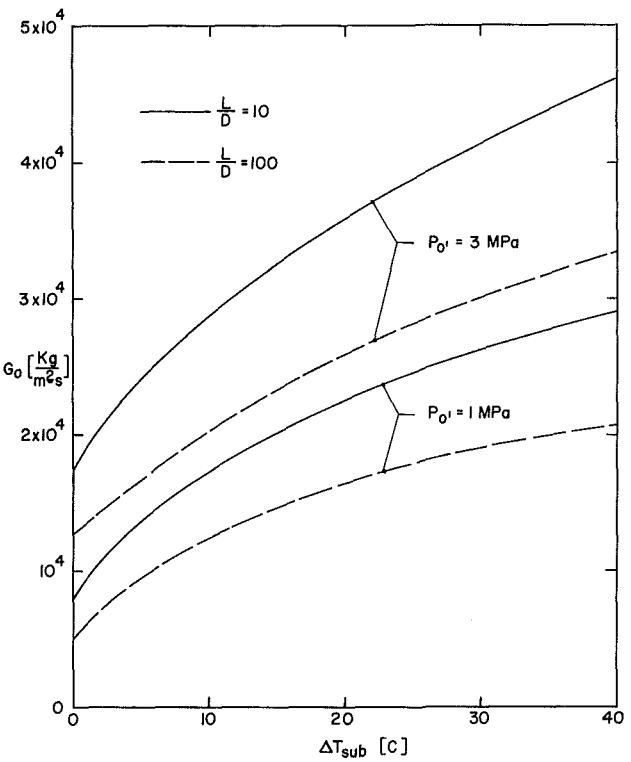

Fig. 9 Relationship between the critical mass flux, subcooling, stagnation pressure, and *L/D*

For the case of subcooled liquid at the tube inlet in Fig. 8, the mechanical and thermal nonequilibrium is significantly increased over that for the saturated liquid situation in Fig. 7, and this increases even further with a decrease in the tube length [5].

The predicted critical two-phase flow results for steam–water are illustrated in Fig. 9 in a plot of critical mass flux versus the liquid subcooling in the vessel for varying stagnation pressures of liquid and tube length to diameter ratios. These results show that higher stagnation pressures, larger liquid subcoolings, and smaller *L/D* ratios produce larger critical mass fluxes.

4 Conclusions

A two-phase flow model was developed for the analysis of critical flows in tubes. The model allows for the thermal and mechanical nonequilibrium between the phases and the resulting nonlinear differential equations were solved by a numerical procedure along the tube until the critical flow is achieved at the tube end. A computer program based on this model was also developed and the predictions of the model were tested with the experimental data of subcooled and saturated water discharging through short and long pipes. It is shown that the model gives very good predictions of the critical flow rates and pressure distributions along the tubes. The numerical results show that increasing the liquid subcooling and decreasing the tube length increases the mechanical and thermal nonequilibrium between the phases and that this nonequilibrium may be considerable close to the tube end. The degree of thermal and mechanical nonequilibrium of the two phases exiting from the tube may have a significant influence on the development of the two-phase flow expansion region on the outside of the tube, and a detailed critical flow modeling as presented in the paper is necessary for reliable prediction of such a flow expansion [25]. The comparison of analytical results of two-phase flow jet expansion with the experimental data in [25] also attests to the credibility of the presented critical flow model.

References

1 Wallis, G. B., "Critical Two-Phase Flow," *International Journal of Multiphase Flow*, Vol. 6, 1980, pp. 97–112.

2 Saha, P., "A Review of Two-Phase Steam–Water Critical Flow Models With Emphasis on Thermal Nonequilibrium," NUREG/CR/0417, BNL-NUREG-50907 Report, 1978.

3 Isbin, H. S., "Some Observations on the Status of Two-Phase Critical Flow Models," *International Journal of Multiphase Flow*, Vol. 6, 1980, pp. 131–138.

4 Richter, H. J., "Separated Two-Phase Flow Model: Application to Critical Two-Phase Flow," *International Journal of Multiphase Flow*, Vol. 9, 1983, pp. 511–530.

5 Dobran, F., "Discharge of Two-Phase Critical Flow Through Tubes," Stevens Institute of Technology Report ME-RT-84016, 1984.

6 Henry, R. E., and Fauske, H. K., "The Two-Phase Critical Flow of One Component Mixtures in Nozzles, Orifices and Tubes," ASME JOURNAL OF HEAT TRANSFER, Vol. 93, 1971, pp. 179–187.

7 Giot, M., and Fritte, A., "Two-Phase Two- and One-Component Critical Flows With the Variable Slip Model," *Prog. Heat Mass Transfer*, Vol. 6, 1972, pp. 651–670.

8 Ardron, K. H., "A Two-Fluid Model for Critical Vapor–Liquid Flow," *International Journal of Multiphase Flow*, Vol. 4, 1978, pp. 323–337.

9 Lyczkowski, R. W., and McFadden, J. H., "Calculations of Nonequilibrium Discharge Flow," *Trans. Can. Society of Mechanical Engineers*, Vol. 4, 1976, pp. 159–166.

10 Rivald, W. C., and Travis, J. R., "A Non-equilibrium Vapor Production Model for Critical Flow," *Nuclear Science Engineering*, Vol. 74, 1980, pp. 40–48.

11 Okazaki, N., "Theoretical Study for Accelerating Two-Phase Flow – I, Constant Area Flow," *Bulletin JSME*, Vol. 23, 1980, pp. 536–544.

12 Wallis, G. B., *One Dimensional Two-Phase Flow*, McGraw-Hill, New York, 1969.

13 Collier, J. G., *Convective Boiling and Condensations*, McGraw-Hill, New York, 1981.

14 Dobran, F., "A Two-Phase Fluid Model Based on the Linearized Constitutive Equations," in: *Advances in Two-Phase Flow and Heat Transfer*, S. Kakac and M. Ishii, eds., Martinus Nijhoff Publishers, Vol. 1, 1983, pp. 41–59.

15 Dobran, F., "Constitutive Equations for Multiphase Mixtures of Fluids," *International Journal of Multiphase Flow*, Vol. 10, 1984, pp. 273–305.

16 Bergles, A. E., Collier, J. G., Delhaye, J. M., Hewitt, G. F., and Mayinger, F., *Two-Phase Flow and Heat Transfer in the Power Process Industries*, Hemisphere, Washington, 1981.

17 Dobran, F., "An Acceleration Wave Model for the Speed of Propagation of Shock Waves in a Bubbly Two-Phase Flow," *ASME/JSME Thermal Engineering Joint Conference*, Y. Mori and W. Yang, eds., Vol. 1, 1983, pp. 1–9.

18 Solbrig, C. W., McFadden, J. H., Lyczkowski, R. W., and Hughes, E. D., "Heat Transfer and Friction Correlations Required to Describe Steam-Water Behavior in Nuclear Safety Studies," *AIChE Symposium Series*, Vol. 174, 1978, pp. 100–128.

19 Chisholm, D., "Pressure Gradients Due to Friction During the Flow of Evaporating Two-Phase Mixtures in Smooth Tubes and Channels," *International Journal of Heat and Mass Transfer*, Vol. 16, 1973, pp. 347–348.

20 Alamgir, M. D., and Lienhard, J. H., "Correlation of Pressure Undershoot During Hot-Water Depressurization," ASME JOURNAL OF HEAT TRANSFER, Vol. 103, 1981, pp. 52–55.

21 Ardron, K. H., "A Two-Fluid Model for Critical Vapor-Liquid Flow," *International Journal of Multiphase Flow*, Vol. 4, 1978, pp. 323–337.

22 Boure, J. A., Fritte, A. A., Giot, M. M., and Reocreux, M. L., "Highlight of Two-Phase Critical Flow," *International Journal of Multiphase Flow*, Vol. 3, 1976, pp. 1–22.

23 Celata, G. P., Cumo, M., Farello, G. E., and Incalcaterra, P. C., "Critical Flow of Subcooled Liquid and Jet Forces," in: *Interfacial Transport Phenomena*, J. C. Chen and S. G. Bankoff, eds., ASME, New York, Vol. 109, 1983.

24 Farello, G. E., "Pressure Measurements in Critical Two-Phase Flows," personal communication, Apr. 1984.

25 Dobran, F., "Distribution of Liquid and Gas in a Jet With Phase Change," *International Symposium on Jets and Cavities*, J. H. Kim, O. Furuya, and B. R. Parkin, eds., ASME, New York, 1985.